

### **Construction and Verification of Pourbaix Diagrams for Hydrogen Sulfide Corrosion of Mild Steel**

Jing Ning, Yougui Zheng, Bruce Brown, David Young and Srdjan Nesic  
Institute for Corrosion and Multiphase Technology, Ohio University  
342 West State Street  
Athens, OH, 45701  
USA

#### **ABSTRACT**

In the present study, a comprehensive thermodynamic model, depicted by Pourbaix diagrams, has been developed with the relatively narrow focus on corrosion of mild steel in oil and gas field conditions. This thermodynamic model focuses on predicting the formation of metastable or stable corrosion products in sour environments at elevated temperature up to 250 °C, which includes mackinawite (FeS), greigite (Fe<sub>3</sub>S<sub>4</sub>), the pyrrhotite group (Fe<sub>1-x</sub>S, x = 0 to 0.17) and pyrite (FeS<sub>2</sub>). The model is based on theoretical thermodynamic calculations and data collection from open literature. As known, the appearance of Pourbaix diagram is significantly affected by temperature since thermodynamic properties are highly sensitive to temperature. Therefore, specific corrosion experiments at two different temperatures (25 °C and 80 °C) were designed to compare the predictions of corrosion products made by the Pourbaix diagrams to those formed during experiments. It was observed that the experimental results generally agreed with the predictions made by the Pourbaix diagrams.

**Keywords:** *Hydrogen sulfide, iron sulfide, Pourbaix diagram, polymorphous, H<sub>2</sub>S corrosion, thermodynamic*

#### **INTRODUCTION**

Although H<sub>2</sub>S corrosion of mild steel has been studied for over 60 years, the mechanisms of uniform H<sub>2</sub>S corrosion have been better understood in the recent decade<sup>1-6</sup>. It is broadly agreed that the formation of an iron sulfide layer on the steel surface plays an essential role in the corrosion of the steel underneath. Many researchers<sup>7-9</sup> have reported a significant decrease in corrosion rate after the formation of the protective iron sulfide layer in a sour environment. Hence, in order to make an accurate prediction of the corrosion rate, the mechanisms related to the formation of the iron sulfide layer need to be better understood.

In many cases of published modeling work, only the mackinawite layer (the initial corrosion product in sour environments) has been considered for a reason of simplicity.<sup>4,5</sup> However, polymorphous iron sulfides such as greigite, pyrrhotite, troilite, and pyrite have been found in facilities containing H<sub>2</sub>S in the oil and gas industry.<sup>10</sup> Furthermore, these iron sulfides are reported to either retard<sup>7-9</sup> or promote<sup>11</sup>

corrosion due to the different physicochemical nature associated with each one. Menendez *et al.*<sup>12</sup> studied the impact of different phases of iron sulfide deposits, such as mackinawite, pyrrhotite, and troilite on initiation of pitting corrosion in a highly sour environment. It was found that severe localized attack was associated with mackinawite deposits, but not with pyrrhotite and troilite deposits. Therefore, there is a need to investigate the influences of iron sulfide polymorphism on corrosion and incorporate this effect into simulation models.

However, the formation and transformation of the polymorphous iron sulfides are complex processes, which are affected by both thermodynamics and kinetics. A Pourbaix diagram, also known as potential-pH stability diagram, has been frequently used to map out corrosion product stability from a thermodynamic perspective. Accordingly, one can make extremely valuable inferences for practical purposes from a Pourbaix diagram, including developing corrosion mitigation strategies, defining cathodic protection, and designing critical corrosion tests with higher efficiency.<sup>13</sup> In fact, one can find a number of thermodynamic models, in the form of Pourbaix diagrams for sour systems, in both the open literature and among the proprietary commercial packages<sup>14-17</sup>. However, significant discrepancies among these models have been found, which are attributed to variations in the choice of the underlying thermodynamic data, selection of chemical species and chemical reactions considered, and different assumptions adopted for calculations (for example: open system vs. closed system), all this making it harder for corrosion engineers to use them with confidence. Thus, in the present work development of calculations underlying Pourbaix diagrams for mild steel corrosion in H<sub>2</sub>S environments is shown, covering typical conditions seen in oil and gas industry. The diagrams are based on open literature data and are presented in a simple way, making it easier for corrosion engineers to understand and interpret them.

## CONSTRUCTION OF POURBAIX DIAGRAMS FOR AN H<sub>2</sub>S-H<sub>2</sub>O-Fe SYSTEM

It is noteworthy that some important assumptions were made here when constructing Pourbaix diagrams shown below. Only ideal behavior of aqueous solutions has been considered in the present work, for reasons of simplicity. Also, only an open system is considered in this study, meaning that the partial pressure of H<sub>2</sub>S is considered to be constant across the whole pH range (and needs to be given as an input value).

### Thermodynamic Background

Since thermodynamic properties are very sensitive to temperature, but relatively insensitive to pressure<sup>13</sup>, the effect of increasing pressure on thermodynamic properties is neglected in this study. Therefore, the Gibbs energy of formation for species at elevated temperature,  $G_{T,P}^o$ , is calculated following Equation (1), which is a temperature dependent function of Gibbs energy of formation at 298.15 K,  $G_{298.15}^o$ , heat capacity,  $C_p$ , and standard molar entropy at 298.15 K,  $S_{298.15}^o$ .

$$G_{T,P}^o = G_{298.15}^o + \int_{298.15}^T C_p dT - T \int_{298.15}^T \frac{C_p}{T} dT - (T - 298.15) \cdot S_{298.15}^o \quad (1)$$

The Gibbs energy of formation and standard molar entropy for most species at reference temperature can be found in the open literature. The heat capacity of various species can be predicted as a function of temperature by using Equation (2):

$$C_p = a + bT + cT^{-2} + dT^2 + eT^{-0.5} \text{ J / mol / K} \quad (2)$$

Where,  $a, b, c, d, e$  are constants that can be found in open literature. It should be noted that the Gibbs energy for the electron is also considered in this work. Since the Gibbs energy of formation for aqueous

H<sup>+</sup> is defined to be zero at any temperature<sup>18,19</sup>, the Gibbs energy for the electron is considered to be half of Gibbs energy for hydrogen gas, shown by Equation (3):<sup>18, 20</sup>

$$G(e) = 0.5G(H_2) \quad (3)$$

### Thermodynamic Data

The standard Gibbs energy at 25°C,  $G_{298.15}^\circ$ , for all species considered in the H<sub>2</sub>S-H<sub>2</sub>O-Fe system has been compiled and presented in the previous study<sup>21</sup>. In the present work, two other thermodynamic properties, the standard molar entropy ( $S_{298.15}^\circ$ ) and heat capacity ( $C_p$ ), are needed for all the species considered in the H<sub>2</sub>S-H<sub>2</sub>O-Fe system. For most of the species, thermodynamic data are mainly collected from literature. However, thermodynamic properties for mackinawite and greigite cannot be found in literature, because these two compounds are not thermodynamically stable, thereby, making experimental measurements hard to perform. Therefore, the heat capacities for these two species are estimated on the basis of other metal sulfides. Likewise, the entropies for mackinawite and greigite are estimated by following the principle proposed by F. Gronvold and E. F. Westrum<sup>22</sup>, which is to estimate the entropy of a compound by combining the cationic entropy contribution and anionic entropy contribution.

In addition, it should be emphasized that both stoichiometric troilite (FeS) and pyrrhotite (Fe<sub>0.877</sub>S) are considered to be part of the pyrrhotite group (Fe<sub>1-x</sub>S, x = 0 to 0.17) in the present work because of the similarity of thermodynamic data. It is acknowledged that the phase transition of troilite and pyrrhotite (i.e. alpha, beta, and gamma) affects the heat capacity, hence, specific heat capacities are used for each phase in this study.

### Pourbaix Diagrams

The Pourbaix diagrams for an H<sub>2</sub>S-H<sub>2</sub>O-Fe system were constructed in a stepwise fashion, from a simple system to a more complicated system. The electrochemical and chemical reactions considered for the H<sub>2</sub>O-Fe system and the H<sub>2</sub>S-H<sub>2</sub>O-Fe system are listed in the previous study<sup>21</sup>.

#### Pourbaix Diagram for a H<sub>2</sub>O-Fe System

As a starting point, a well known Pourbaix diagram for an H<sub>2</sub>O-Fe system generated at a specific condition is shown in Figure 1. The areas of “Fe(OH)<sub>2</sub>”, “Fe<sub>2</sub>O<sub>3</sub>”, and “Fe<sub>3</sub>O<sub>4</sub>” indicate the formation of a certain corrosion product layer, but do not indicate how this layer affects corrosion. The protectiveness of the formed layer depends on its adherence to the steel surface, thickness, porosity, tortuosity, and physicochemical properties such as crystal structure and defects, which are related to kinetics of formation.<sup>23</sup>

#### Pourbaix Diagram for an H<sub>2</sub>S-H<sub>2</sub>O-Fe System

To construct Pourbaix diagrams for an H<sub>2</sub>S-H<sub>2</sub>O-Fe system, the reactions of formation of mackinawite (FeS), greigite (Fe<sub>3</sub>S<sub>4</sub>), the pyrrhotite group (FeS) and pyrite (FeS<sub>2</sub>) are incorporated into the Pourbaix diagram for the H<sub>2</sub>O-Fe system. Consequently, Pourbaix diagrams for H<sub>2</sub>S-H<sub>2</sub>O-Fe system with addition of mackinawite, greigite, the pyrrhotite group, and pyrite are shown in Figure 2 (a), (b), (c), and (d), respectively, and are indicated by the black lines. Only pyrrhotite and pyrite exist in the Pourbaix diagram which considers all four iron sulfides in Figure 2 (d), suggesting that these two phases of iron sulfide are the final and thermodynamically stable iron sulfides.

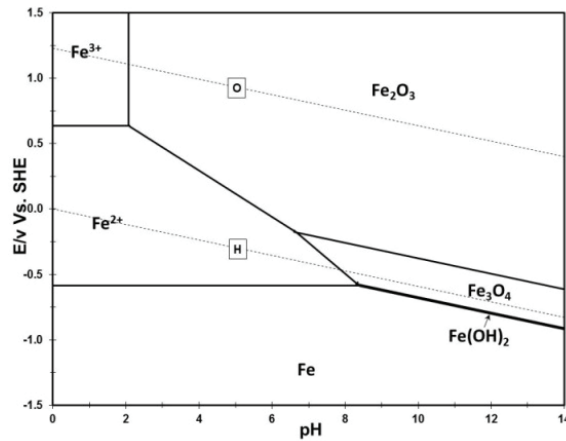


Figure 1. Pourbaix diagram for H<sub>2</sub>O-Fe system (T = 25 °C, [Fe<sup>2+</sup>] = 10 ppm, [Fe<sup>3+</sup>] = 10<sup>-6</sup> mol/L, p<sub>H<sub>2</sub></sub> = p<sub>O<sub>2</sub></sub> = 1 bar).

## Parametric Study

The effects of increasing temperature, ferrous ion concentration in solution, and H<sub>2</sub>S partial pressure on features of Pourbaix diagrams for H<sub>2</sub>S-H<sub>2</sub>O-Fe system are described below.

### Effect of Temperature

Since thermodynamic properties are highly sensitive to temperature, the Pourbaix diagrams for H<sub>2</sub>S-H<sub>2</sub>O-Fe system generated at 25 °C, 80 °C, 150 °C, and 250 °C are presented in Figure 2 using the colored lines. In order to compare Pourbaix diagrams among different temperatures in a reasonable way, the dissolved H<sub>2</sub>S concentration in aqueous solution is maintained at a constant level (9.4 x 10<sup>-3</sup> mol/L) during the construction of the series of Pourbaix diagrams.

A gradual shift of the stability areas for formed solids to lower pH and to more negative potential with increasing temperature is clear in Figure 2. This indicates that higher temperatures are more thermodynamically favorable for the formation of a corrosion product layer, such as iron sulfides and hematite, possibly retarding corrosion rate of steel underneath. Abayarathna *et al.*<sup>24</sup> conducted steel corrosion tests with continuous purge of pure H<sub>2</sub>S gas into brine at 50 °C, 70 °C, and 90 °C for two days of exposure. The results show the final corrosion rate at 90 °C was much lower than that at 50 °C due to the formation of the more protective iron sulfide layer at 90 °C.

In addition, the type of the corrosion product formed was also affected by changing temperature. In Figure 2 (b) and (c), greigite is predicted to be the main corrosion product at 25 °C through 200 °C, but not at 250 °C. At 250 °C, greigite is completely replaced by hematite since hematite is more stable than greigite at 250 °C.

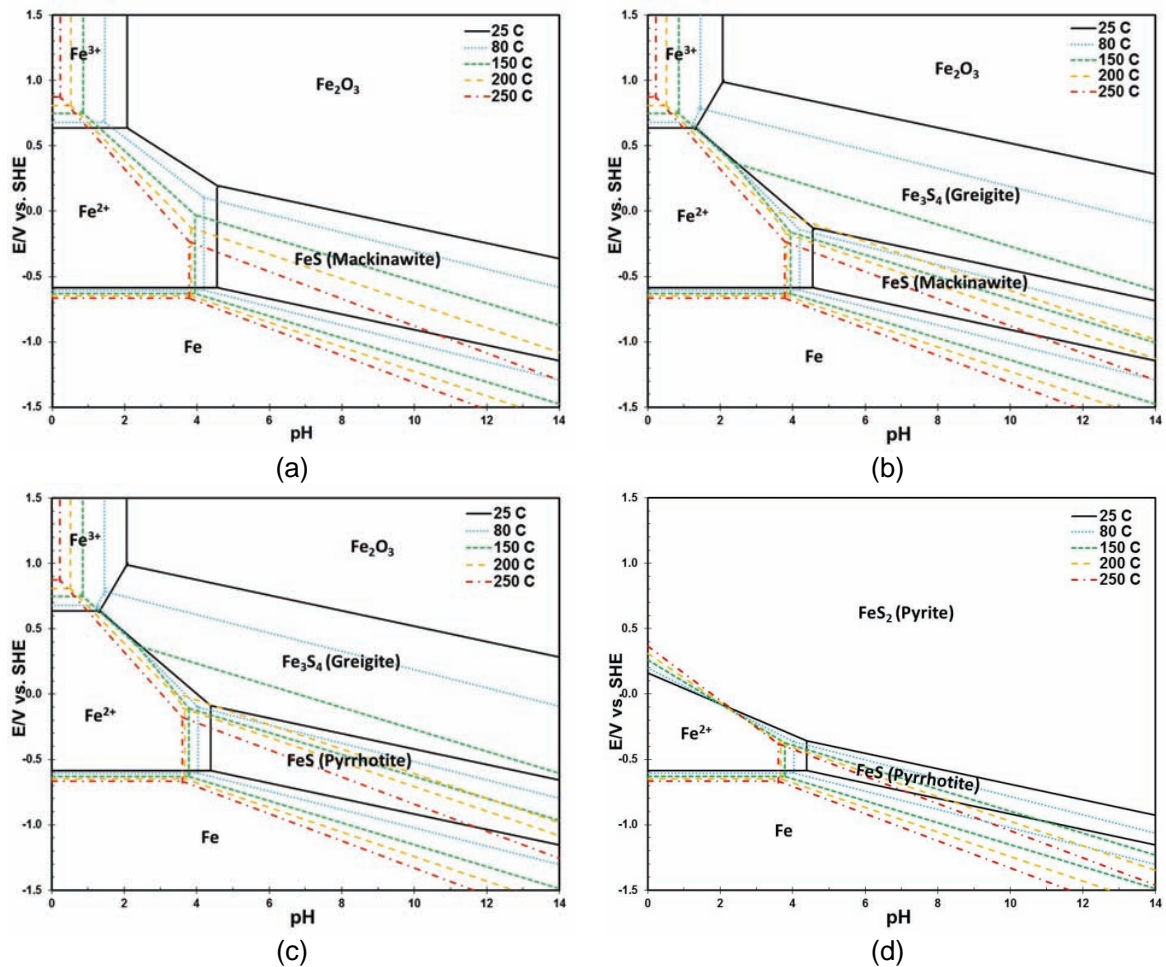


Figure 2. Pourbaix diagrams for  $\text{H}_2\text{S}$ - $\text{H}_2\text{O}$ - $\text{Fe}$  system showing step changes in temperature up to  $250^\circ\text{C}$  ( $T = 25^\circ\text{C} - 250^\circ\text{C}$ ,  $[\text{H}_2\text{S}]_{\text{aq}} = 9.4 \times 10^{-3} \text{ M}$ ,  $[\text{Fe}^{2+}] = 10 \text{ ppm}$ ,  $[\text{Fe}^{3+}] = 10^{-6} \text{ M}$ ): (a) Mackinawite; (b) Mackinawite / Greigite; (c) Mackinawite / Greigite / Pyrrhotite; (d) Mackinawite / Greigite / Pyrrhotite / Pyrite.

### Effect of $\text{H}_2\text{S}$ Partial Pressure

Variation of another significant factor, partial pressure of  $\text{H}_2\text{S}$ , is also considered here. The Pourbaix diagrams are developed for partial pressure of  $\text{H}_2\text{S}$  at 0.0001 bar (100 ppm at atmospheric pressure), 0.1 bar, 1 bar, and 10 bar and shown in Figure 3.

A major effect of increasing partial pressure of  $\text{H}_2\text{S}$  on the features of Pourbaix diagrams is the expansion of corrosion product layer stability region, particularly that of iron sulfide. Since mackinawite usually forms as the initial and main corrosion product in  $\text{H}_2\text{S}$  corrosion and provides some protectiveness, the understanding of conditions leading to establishment of mackinawite layer is critical to short term corrosion studies. Figure 3 (a) shows that the increase in  $\text{H}_2\text{S}$  partial pressure from 0.0001 bar to 10 bar dramatically pushes the boundary of mackinawite formation region from pH 6.0 to pH 3.3, revealing the formation of mackinawite layer is more thermodynamically favored at higher  $\text{H}_2\text{S}$  partial pressure.

Furthermore,  $\text{Fe}_3\text{O}_4$  is seen in the presence of trace amounts of  $\text{H}_2\text{S}$  (0.0001 bar) but is replaced by iron sulfides at higher concentrations of  $\text{H}_2\text{S}$ , as shown in Figure 3 (a), (b), and (c).

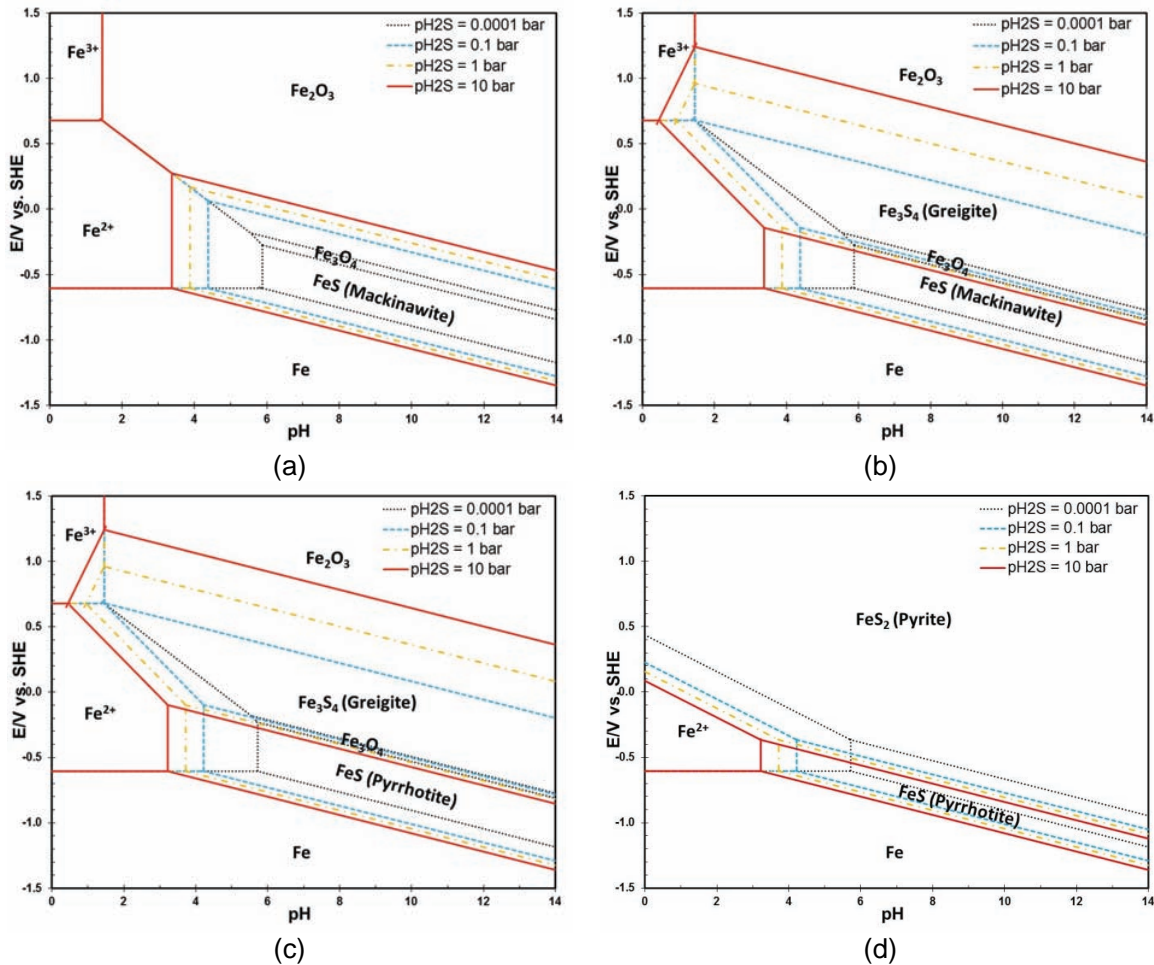


Figure 3. Pourbaix diagrams for H<sub>2</sub>S-H<sub>2</sub>O-Fe system showing step changes in H<sub>2</sub>S partial pressure (pH<sub>2</sub>S = 0.0001 – 10 bar, T = 80 °C, [Fe<sup>2+</sup>] = 10 ppm, [Fe<sup>3+</sup>] = 10<sup>-6</sup> M): (a) Mackinawite; (b) Mackinawite / Greigite; (c) Mackinawite / Greigite / Pyrrhotite; (d) Mackinawite / Greigite / Pyrrhotite / Pyrite.

### Effect of Ferrous Ion Concentration

The concentration of ferrous ion in solution directly affects the saturation value for iron sulfide. Sun *et al.*<sup>25</sup> concluded that the effect of ferrous ion concentration on H<sub>2</sub>S corrosion rate is negligible since the solubility of iron sulfide is so small that supersaturation for iron sulfide can be easily reached.

Figure 4 shows a series of Pourbaix diagrams developed with 1 ppm, 10 ppm, and 100 ppm ferrous ion concentration. Notice that the “Fe<sup>2+</sup>” area shrinks with increasing ferrous ion concentration, which is considered to be an indication that bare steel corrosion is less likely. However, the increase in size of the iron sulfide stability area does not necessarily guarantee better protectiveness of the formed iron sulfide layer, which is more related to the kinetics aspects.

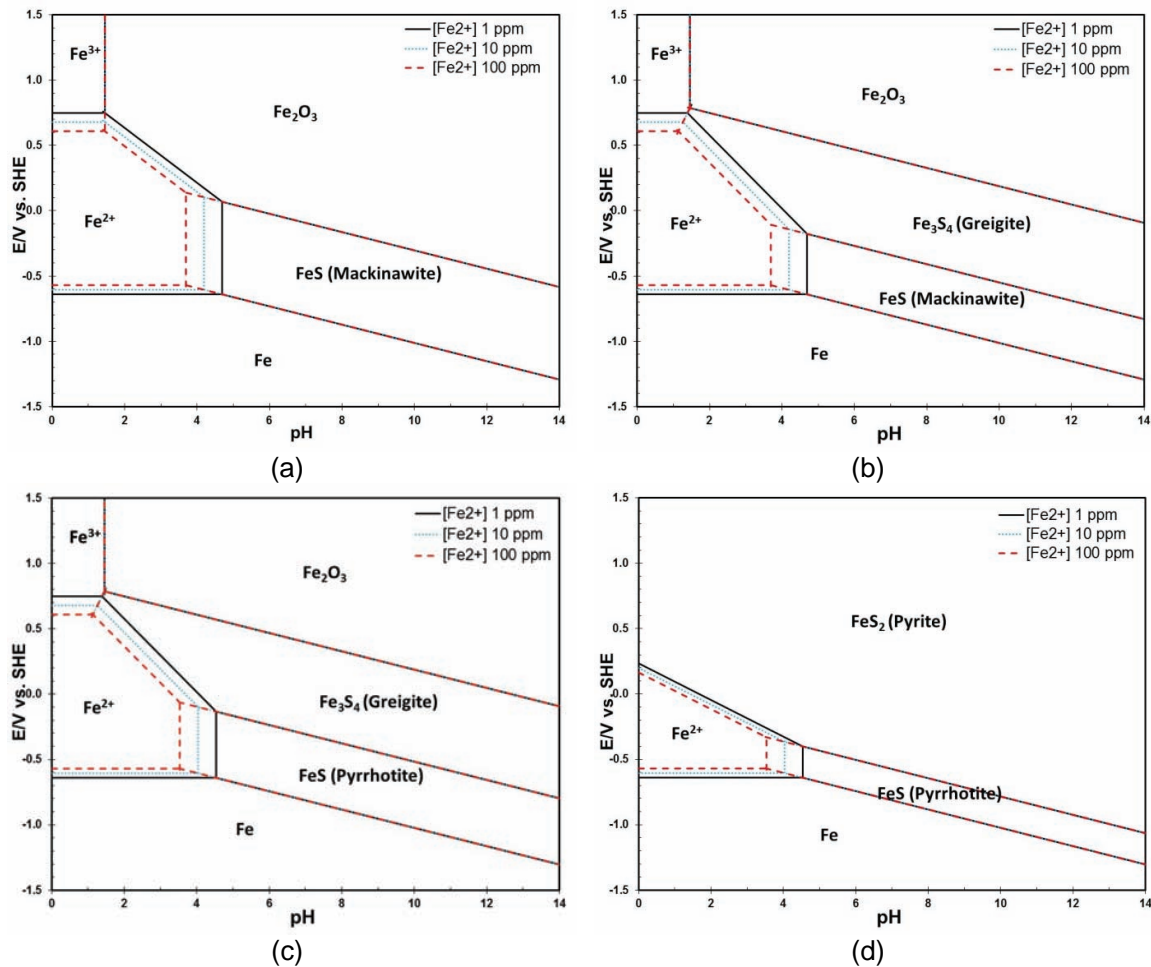


Figure 4. Pourbaix diagrams for  $\text{H}_2\text{S}$ - $\text{H}_2\text{O}$ - $\text{Fe}$  system showing step changes in ferrous ion concentration ( $[\text{Fe}^{2+}] = 1\text{-}100$  ppm,  $T = 80$  °C,  $\text{pH}_{\text{H}_2\text{S}} = 0.24$  bar,  $[\text{Fe}^{3+}] = 10^{-6}$  M): (a) Mackinawite; (b) Mackinawite / Greigite; (c) Mackinawite / Greigite / Pyrrhotite; (d) Mackinawite / Greigite / Pyrrhotite / Pyrite.

## EXPERIMENTAL VERIFICATION OF CONSTRUCTED POURBAIX DIAGRAMS

A comprehensive thermodynamic model for the  $\text{H}_2\text{S}$ - $\text{H}_2\text{O}$ - $\text{Fe}$  system, in the form of Pourbaix diagrams, was described in the section above with the relatively narrow focus on predicting corrosion products for environments similar to those found in the oil and gas fields. After the establishment of the theoretical model, verification of the Pourbaix diagrams is required by performing experiments. It is notoriously difficult to verify Pourbaix diagrams due to a variety of theoretical and practical limitations.

First, thermodynamics is a science related to the equilibrium state defined by thermodynamic state variables, which are independent on the path and the history (time) of the system. To be more specific, for given conditions of pH and potential, a specific iron sulfide is predicted to form by the Pourbaix diagram, but how that iron sulfide forms and how long it takes to form are unknown. Considering the stabilities of four different kinds of iron sulfides makes this thermodynamic model more complex and harder to verify. Moreover, in reality, most systems are transient, which means they are not in thermodynamic equilibrium and are gradually changing over time. In the present study, two long-term corrosion tests at two different temperatures (25 °C and 80 °C) were performed to test the corrosion product stability predictions by the Pourbaix diagrams, and especially to compare the equilibrium state

(given by the line) in the Pourbaix diagram with the quasi-equilibrium state attained in long-term experiments.

In addition, there is another experimental challenge and that is to accurately determine pH and ferrous ion concentration at the steel surface, which can be very different from those in the bulk. In the present work, a mesh capped flat pH probe<sup>26</sup> was used for improved estimation of surface pH. The measured ferrous ion concentration in the bulk solution in well mixed conditions was used to approximate the surface ferrous ion concentration.

## Experimental

### Apparatus

The experimental setup is depicted in Figure 5. Experiments were carried out in a 2-liter glass cell filled with 1 wt. % sodium chloride (NaCl) electrolyte at atmospheric pressure. Square samples were suspended in the glass cell. One rotating cylinder electrode (RCE) sample was used as the working electrode to conduct electrochemical measurements, but was not rotated during the experiment. A platinum wire was used as the counter electrode. A saturated silver-silver chloride (Ag / AgCl) electrode connected to the cell externally through a Luggin capillary was used as the reference electrode. The open circuit potential (OCP) of the RCE electrode was monitored using a potentiostat. A magnetic stirring bar with 400 rpm stirring speed was used to mix solution during the experiment. A mesh capped pH probe was used to measure surface pH at steel mesh surface and a regular pH probe was used to monitor bulk solution pH as well. The concentration of H<sub>2</sub>S in the mixed H<sub>2</sub>S/N<sub>2</sub> gas was adjusted by using a gas rotameter and confirmed by a gas sample pump with H<sub>2</sub>S detector tubes. Sodium hydroxide solution and a carbon scrubber were used to remove H<sub>2</sub>S from the gas coming out of the glass cell.

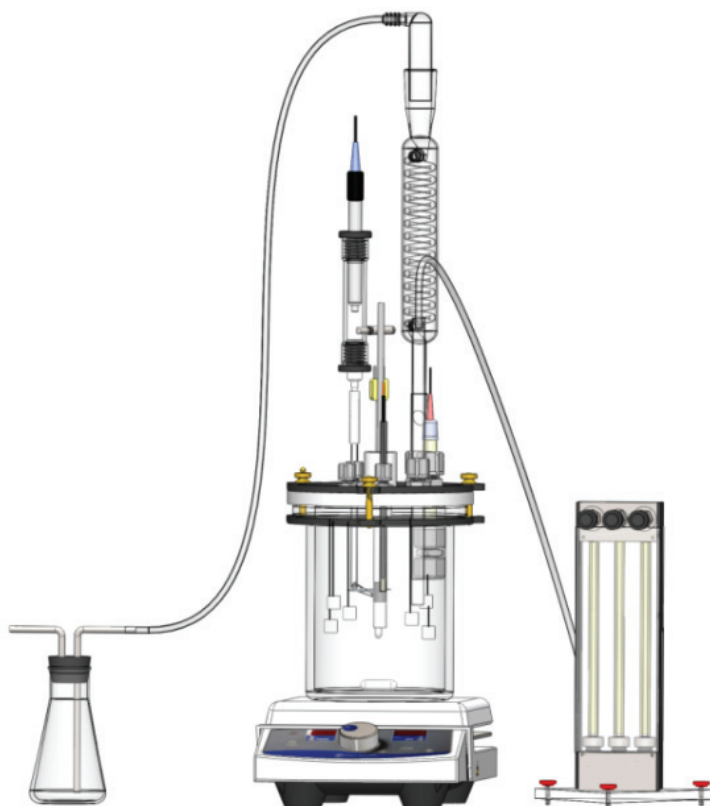


Figure 5. Experimental setup.

## **Material**

The square samples with 1.2 cm x 1.2 cm x 0.2 cm dimension and the RCE sample with an exposed area of 5.4 cm<sup>2</sup> were machined from API<sup>(1)</sup> 5L X65 carbon steel. The chemical composition of this type of carbon steel is presented in Table 1.

Table 1 Chemical composition of 5L X65 carbon steel used in experiment (wt. %).

Cr	Mo	S	V	Si	C	Fe	Ni	Mn	P
0.14	0.16	0.009	0.047	0.26	0.13	Balance	0.36	1.16	0.009

## **Procedure**

The test matrix is shown in Table 2. The experiments were conducted with 10% H<sub>2</sub>S in the gas phase at 25 °C and 80 °C, corresponding to a H<sub>2</sub>S partial pressure of 0.097 bar at 25 °C and 0.053 bar at 80 °C. Prior to a test, N<sub>2</sub> gas was purged into the electrolyte until saturation to deoxygenate the solution (typically more than 4 hours). An H<sub>2</sub>S and N<sub>2</sub> pre-mixed gas was then purged into the solution until the solution pH stabilized and was purged continuously throughout the experiment. Before positioning steel samples in the glass cell, the solution pH was adjusted to 6.0 by using deoxygenated NaOH solution. The RCE sample and square samples were finally polished with 600 grit sandpaper, rinsed thoroughly with deionized water and isopropanol before immersion in solution. Corroded square samples were taken out for analysis at different points in time, rinsed with deoxygenated DI water and deoxygenated isopropanol, blown dry using N<sub>2</sub>, and stored in desiccator. Scanning Electron Microscope (SEM) imaging was used to detect the surface morphologies of the square samples. X-ray Diffraction (XRD) was applied to determine which iron sulfides formed on the square samples. Both Linear Polarization Resistance (LPR) and weight loss methods were adopted for corrosion rate measurements. Approximately 10 ml of solution was drawn from glass cell immediately before taking each steel specimen, filtered by using a 0.22 μm syringe filter to remove any iron sulfide precipitate from solution, and then taken for the measurement of ferrous ion concentration using a spectrophotometric method.

Table 2 Test matrix.

Description	Parameter
Temperature	25 °C, 80 °C
Solution	1 wt.% NaCl brine
Purge gas	10% H <sub>2</sub> S/balance N <sub>2</sub>
H <sub>2</sub> S partial pressure	0.097 bar (25 °C), 0.053 bar(80 °C)
Stirring speed	400 rpm
Material	API <sup>(1)</sup> 5L X65

## **Results and Discussion**

### **Verification of Pourbaix diagram for H<sub>2</sub>S-H<sub>2</sub>O-Fe system at 25 °C**

To verify the basis of this thermodynamic model, the first corrosion test was performed at 25 °C. Figure 6 (a) shows the surface pH, bulk pH, and the ferrous ion concentration in the bulk solution changing over time. One can observe that the surface pH is approximately 0.5 pH unit higher than the bulk pH in the initial three days, which reflects the rapid release of Fe<sup>2+</sup> ions and consumption of hydrogen ions in the corrosion reaction. After three days, the surface pH becomes lower than the bulk pH, which is due to the release of hydrogen ions (acidification) during precipitation of iron sulfide. Figure 6 (b) shows that both corrosion rate and OCP had small changes in the first day and then were very stable through the seven days of the experiment.

<sup>(1)</sup> American Petroleum Institute (API), 1220 L Street, NW, Washington, DC 20005-4070

At the time each square sample was removed from the cell for the determination of corrosion product composition, a set of operational parameters was determined and used to define the “operational point” in the Pourbaix diagram. This includes the values of OCP and surface pH, ferrous ion concentration, H<sub>2</sub>S partial pressure, and temperature.

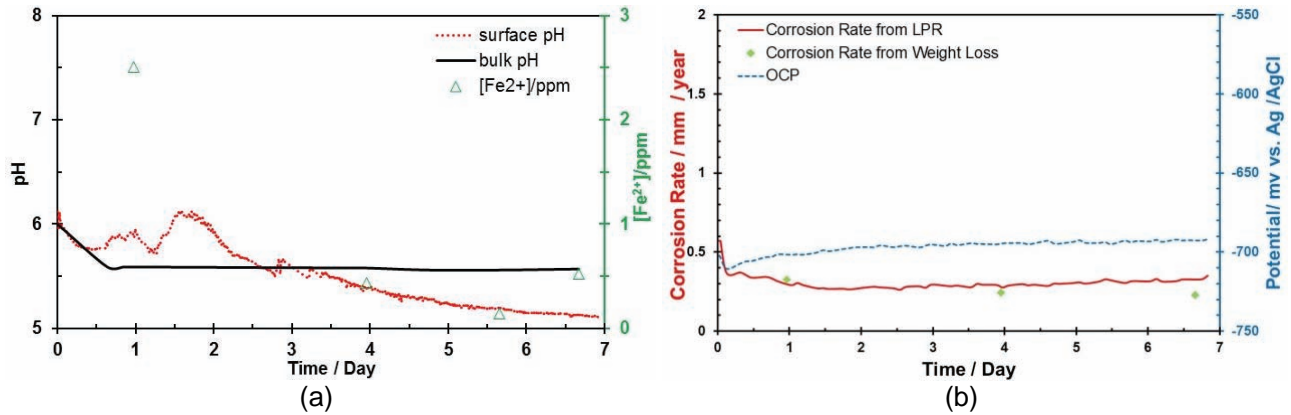


Figure 6. (a) Measured bulk pH, surface pH, and [Fe<sup>2+</sup>]; (b) Corrosion rate and OCP during experiment at 25 °C.

### Results after 1 day of exposure

Figure 7 (a), (b) show the surface morphologies of the sample after one day of exposure. A partially covered corrosion product layer is observed on the surface, and is identified to be only mackinawite by XRD, as shown in Figure 7 (c).

Figure 8 shows the Pourbaix diagram constructed at this experimental condition, which considers only mackinawite corrosion product and excludes other polymorphous iron sulfides. According to the intersection of potential and surface pH from measurement in Figure 8, mackinawite is predicted to form on the steel surface, which is detected in experiment as well.

Moreover, the operational point is a little to the right of the equilibrium line between mackinawite and aqueous Fe<sup>2+</sup>, which indicates a slight supersaturation for mackinawite (a non-equilibrium state) at this condition. This statement is quantified by calculating the saturation value for mackinawite, using Equation (4), which gives  $S = 20$ . This could be an experimental artifact resulting from the errors made in estimating the surface pH and ferrous ion concentration, but it could also be true – indicating that kinetics of mackinawite formation at 25 °C lags behind the corrosion process. If the latter is true, as time progresses, one would expect the saturation value to decrease and the intersection of potential and surface pH to be closer to the equilibrium line, which is exactly what is seen in the results collected after 4 days and 7 days of exposure (see below).

$$S_{Mackinawite} = \frac{c_{Fe^{2+}} \cdot c_{HS^-}}{K_{sp,2} \cdot c_{H^+}} = 20 \quad (4)$$

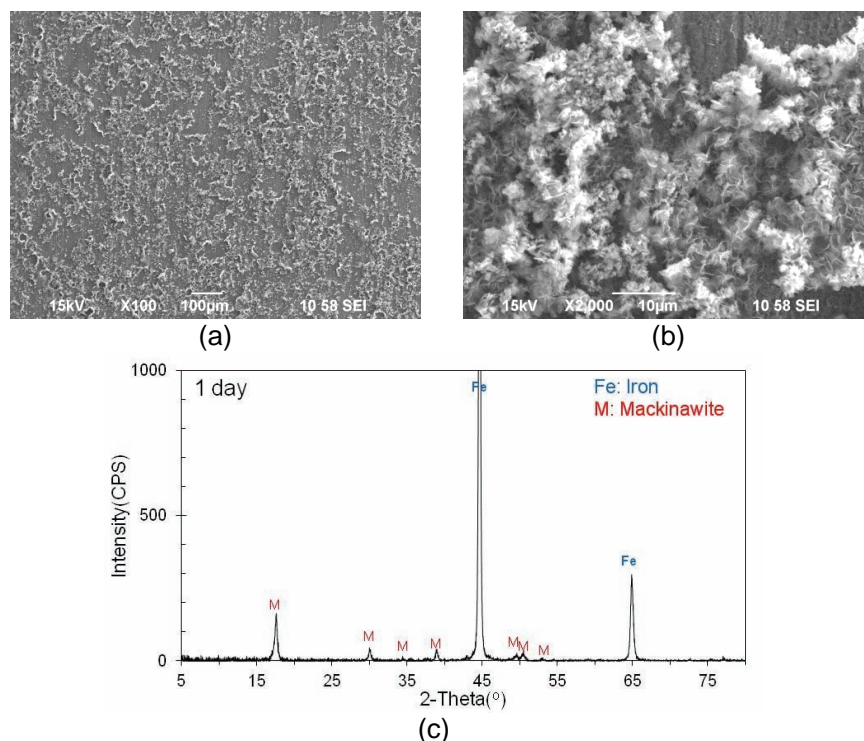


Figure 7. Corrosion product layer after 1 day of exposure at 25°C: (a) Surface morphology with x 100 magnification; (b) Surface morphology with x 2,000 magnification; (c) XRD pattern.

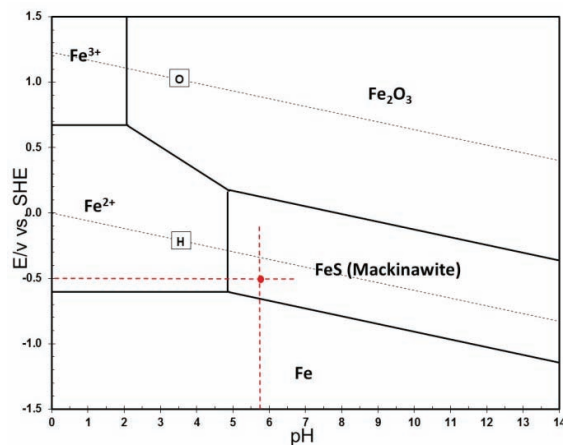


Figure 8. Verification of Pourbaix diagram after 1 day of exposure (Pourbaix diagram was generated at T = 25 °C, p<sub>H<sub>2</sub>S</sub> = 0.097 bar, [Fe<sup>2+</sup>] = 2.5 ppm, [Fe<sup>3+</sup>] = 1.0 x 10<sup>-6</sup> M).

### Results after 4 days of exposure

Figure 9 presents the surface morphology and compositional analysis of the corrosion product layer on the steel surface after 4 days of exposure. A steel surface covered with more corrosion product layer is observed in Figure 9 (a). SEM image at higher magnification (Figure 9 (b)) shows this corrosion product to be in the form of “plates” and some slender needle-like clusters. XRD pattern in Figure 9 (c) suggests the presence of mackinawite with a small amount of pyrrhotite. According to the Pourbaix diagrams constructed at this experimental condition shown in Figure 10, the expected corrosion products are mackinawite and pyrrhotite, which are both detected by XRD. The dominant corrosion product, mackinawite, is a thermodynamic metastable phase which forms first because of its faster kinetics. It will transform to a thermodynamically more stable phase, pyrrhotite or pyrite, over time. However, the

time of this transformation cannot be depicted in the Pourbaix diagram, and two different Pourbaix diagrams are shown in Figure 10.

Furthermore, comparing with the previous results collected after one day of exposure, the operational point in Figure 10 (a) is much closer to equilibrium line for mackinawite, and the saturation value is 2. This implies that the system is approaching the equilibrium for formation of mackinawite. The operational point in the Pourbaix diagram showing pyrrhotite, Figure 10 (b) is further to the right of the equilibrium line, suggesting a slower kinetics of formation.

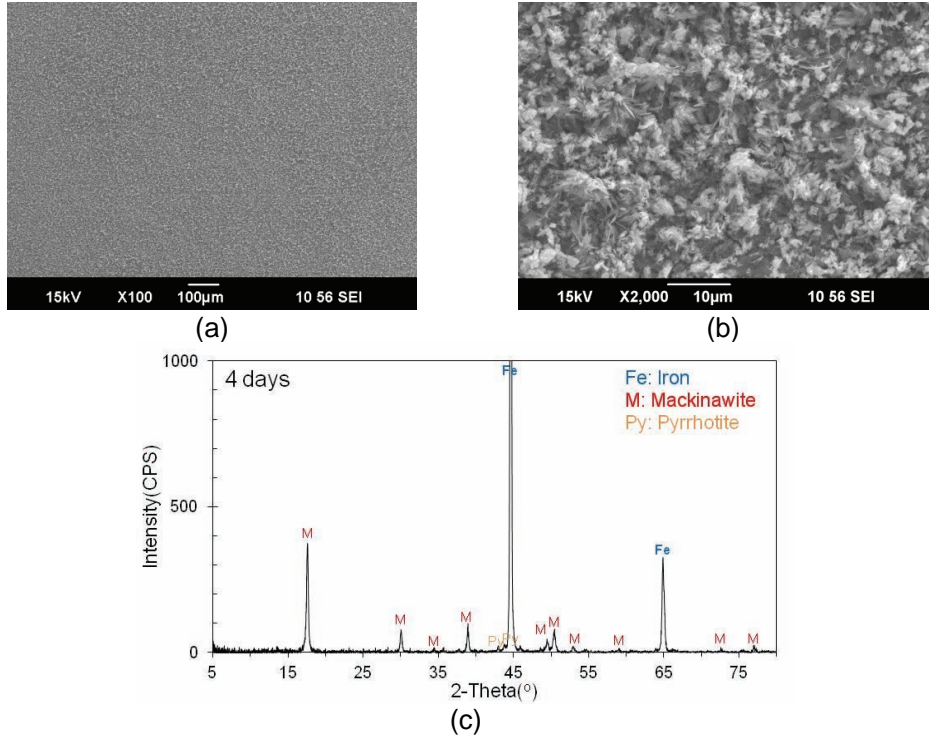


Figure 9. Corrosion product layer after 4 days of exposure at 25°C: (a) SEM image of surface morphology with x 100 magnification; (b) SEM image of surface morphology with x 2,000 magnification; (c) XRD pattern.

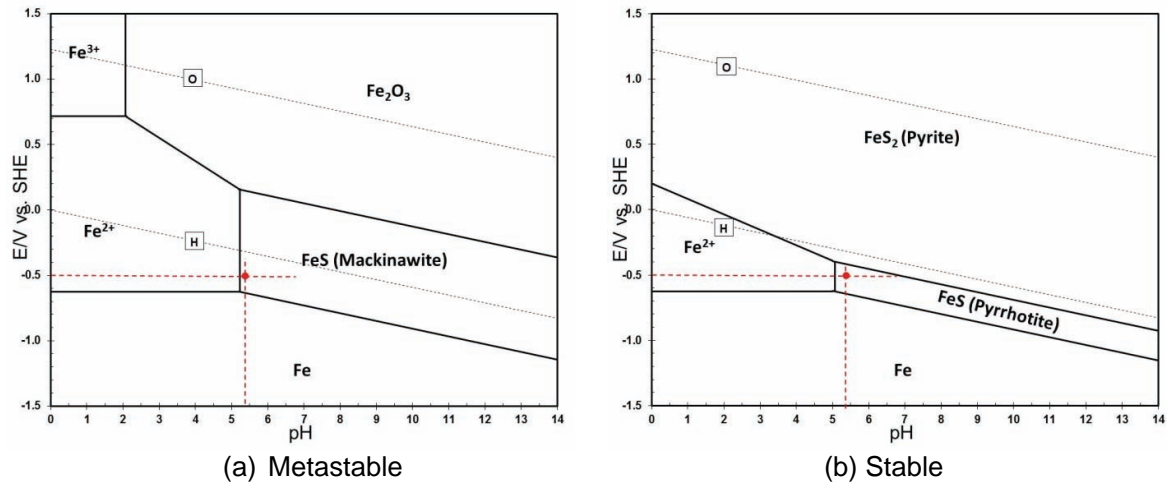


Figure 10. Verification of Pourbaix diagram after 4 days of exposure (Pourbaix diagram was generated at T = 25 °C, p<sub>H<sub>2</sub>S</sub> = 0.097 bar, [Fe<sup>2+</sup>] = 0.44 ppm, [Fe<sup>3+</sup>] = 1.0 x 10<sup>-6</sup> M): (a) Mackinawite; (b) Mackinawite / Greigite / Pyrrhotite / Pyrite.

## Results after 7 days of exposure

Figure 11 demonstrates the morphology and composition of corrosion product layer on the steel surface after corroding for 7 days. The SEM image with x 100 magnification shows a fully covered steel surface. The SEM image with higher magnification presents a mixture flaky crystals and needle-like clusters. Again, mackinawite and pyrrhotite were detected by XRD with mackinawite as the dominate polymorph. Referring to the Pourbaix diagrams generated at this experimental condition (Figure 12), mackinawite and pyrrhotite are predicted as stable, which were also detected in the experiment.

In addition, the operational point is almost on the equilibrium line between mackinawite and ferrous ion in Figure 12 (a), which indicates, that after long-term exposure for 7 days, the system finally reached a state very close to the equilibrium between mackinawite precipitation and dissolution, which is here called quasi-equilibrium. The saturation value for mackinawite after 7 days of test was computed to be 0.7. The operational point in the Pourbaix diagram showing pyrrhotite given in Figure 12 (b) is also closer to the equilibrium line suggesting that the formation of pyrrhotite also approached equilibrium after 7 days of exposure at 25 °C. The consistency of these results presents credible evidence in favor of the accuracy of the current thermodynamic model, at least for 25 °C.

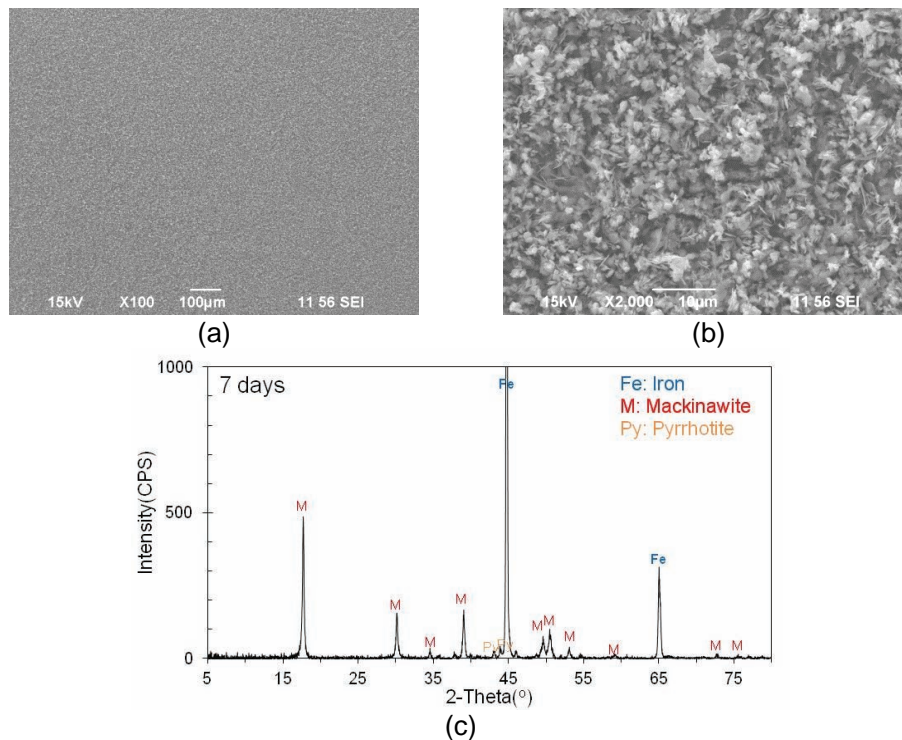


Figure 11. Corrosion product layer after 7 days of exposure at 25°C: (a) SEM image of surface morphology with x 100 magnification; (b) SEM image of surface morphology with x 2,000 magnification; (c) XRD pattern.

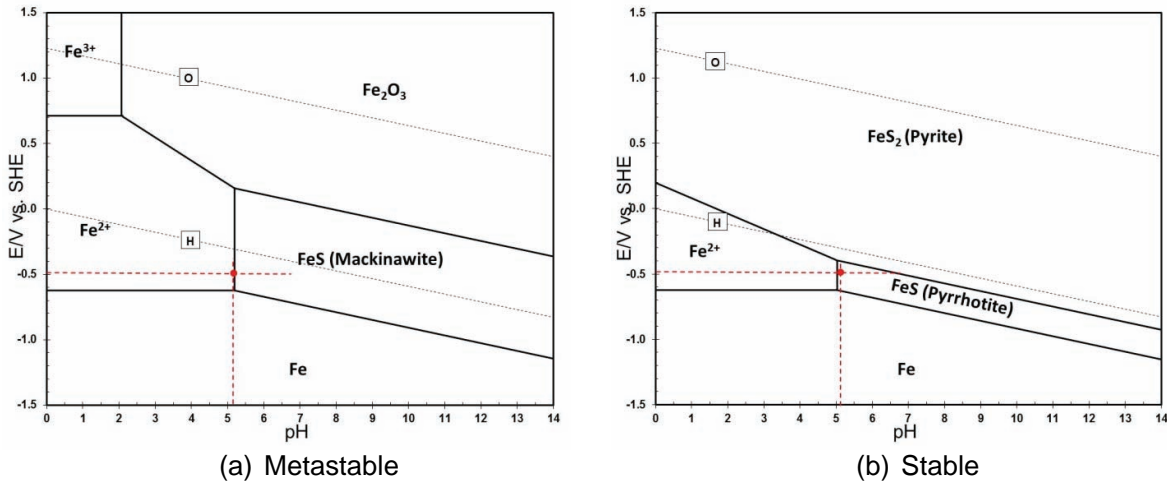


Figure 12. Verification of Pourbaix diagram after 7 days of exposure (Pourbaix diagram was generated at  $T = 25\text{ }^{\circ}\text{C}$ ,  $p\text{H}_2\text{S} = 0.097\text{bar}$ ,  $[\text{Fe}^{2+}] = 0.52\text{ ppm}$ ,  $[\text{Fe}^{3+}] = 1.0 \times 10^{-6}\text{ M}$ ): (a) Mackinawite; (b) Mackinawite / Greigite / Pyrrhotite / Pyrite.

### Verification of Pourbaix diagram for $\text{H}_2\text{S}\text{-H}_2\text{O}\text{-Fe}$ system at $80\text{ }^{\circ}\text{C}$

It is known that increasing temperature facilitates the transformation of the metastable phases: mackinawite or greigite, into more stable phases: pyrrhotite or pyrite. Compared to the low temperature experiments presented above, different phases of iron sulfides should be detected at the high temperature conditions. Moreover, increasing temperature also expedites the kinetics and the approach of the equilibrium state. Therefore, a second set of experiments at higher temperature,  $80\text{ }^{\circ}\text{C}$ , were carried out for verification.

Figure 13 (a) shows the bulk pH monitored and  $[\text{Fe}^{2+}]$  measured through the experiment. Figure 13 (b) demonstrates the evolution of OCP and corrosion rates during the test. The corrosion rate decreased from  $1.1\text{ mm/year}$  to a stable value around  $0.07\text{ mm/year}$  in the first four days probably due to the formation of a protective mackinawite layer, but then increased gradually. A significant change in OCP is observed at the same time. This effect on the corrosion rate is very interesting and could be the effect of other iron sulfide phases forming on the steel surface. However a deeper analysis is currently under way and a full presentation exceeds the scope of the current paper.

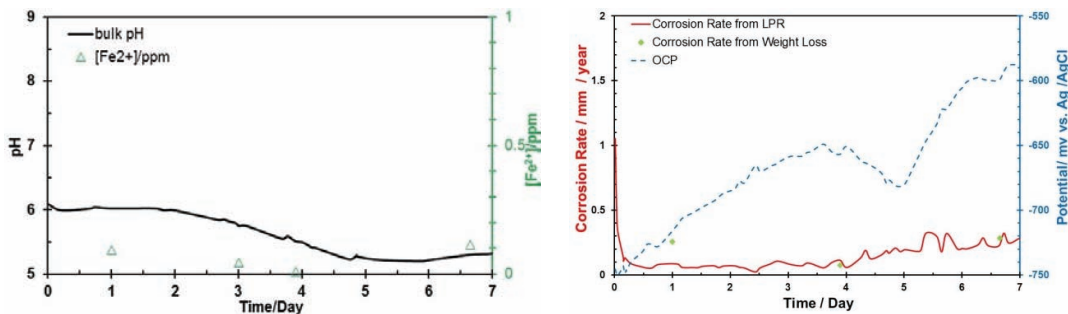


Figure 13. (a) Measured bulk pH and  $[\text{Fe}^{2+}]$ ; (b) Corrosion rate and OCP during experiment at  $80\text{ }^{\circ}\text{C}$ .

### Results after 1 day of exposure

In Figure 14, the SEM images show a uniform corrosion product layer formed on the steel surface after 1 day of exposure, which is characterized to be only mackinawite by XRD. According to the Pourbaix diagram generated at experimental conditions after 1 day in Figure 15, the mackinawite corrosion product is predicted, which matches the experimental results. The operational point is to the right of the

equilibrium line, indicating the system is in non-equilibrium state for mackinawite formation after 1 day of test. The supersaturation value for mackinawite was computed to be 78, which suggests precipitation of mackinawite was not at equilibrium state. Even if precipitation of mackinawite was accelerated at 80 °C, so was the corrosion rate making it difficult to reach equilibrium after only 1 day of exposure.

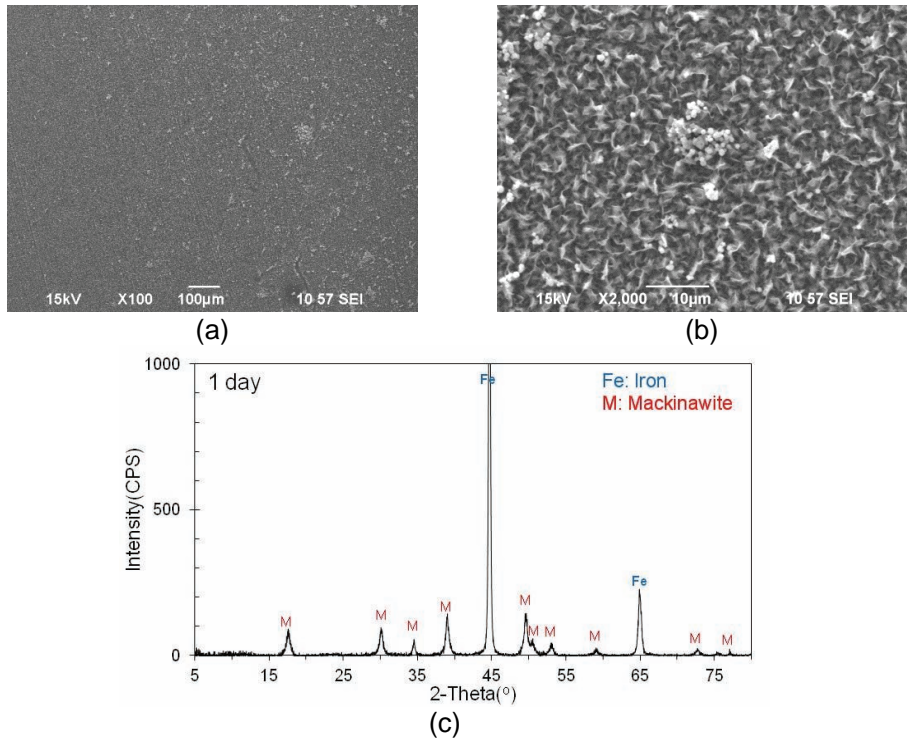


Figure 14. Corrosion product layer after 1 day of exposure at 80 °C: (a) SEM image of surface morphology with x 100 magnification; (b) SEM image of surface morphology with x 2,000 magnification; (c) XRD pattern.

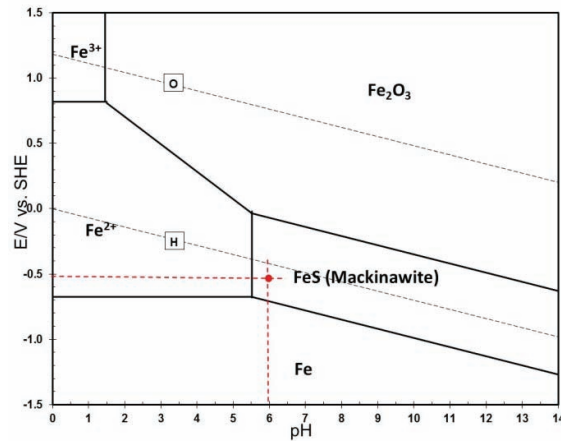


Figure 15. Verification of Pourbaix diagram after 1 day of exposure (Pourbaix diagram was generated at T = 80 °C, pH<sub>2</sub>S = 0.053bar, [Fe<sup>2+</sup>] = 0.1 ppm, [Fe<sup>3+</sup>] = 1.0 x 10<sup>-6</sup> M).

### **Results after 4 days of exposure**

Figure 16 shows the surface morphologies and composition of the corrosion product layer on the sample surface after 4 days of exposure. Figure 16 (b) shows some small cubic crystals on the corrosion product layer, which are suspected to be pyrite. From XRD patterns, beside mackinawite and

pyrrhotite, a new iron sulfide phase is detected as pyrite, which never appeared in the previous experiment at 25 °C. That is because pyrite is a thermodynamic stable phase whose formation is favored by the high temperature in this test. Table 3 gives the quantitative analysis of the formed corrosion products by following Reference Intensity Ratio (RIR) methodology. Mackinawite accounts for 34 % and pyrite makes up 2 % of the total detected layer on the sample surface.

The formation of pyrite is also predicted by the Pourbaix diagram generated according to experimental conditions after 4 days, as shown in Figure 17. From Figure 17 (a), we can see that the operational point is very close to the boundary for mackinawite formation, which indicates the state of quasi-equilibrium for this phase. The fact that the point is slightly to the left of the line (in the undersaturated region) could indicate that mackinawite is gradually been converted into pyrite, although the margin is too small to be certain. The same operational point shown in Figure 17 (b) is very close to the boundary for pyrite formation, confirming the XRD findings.

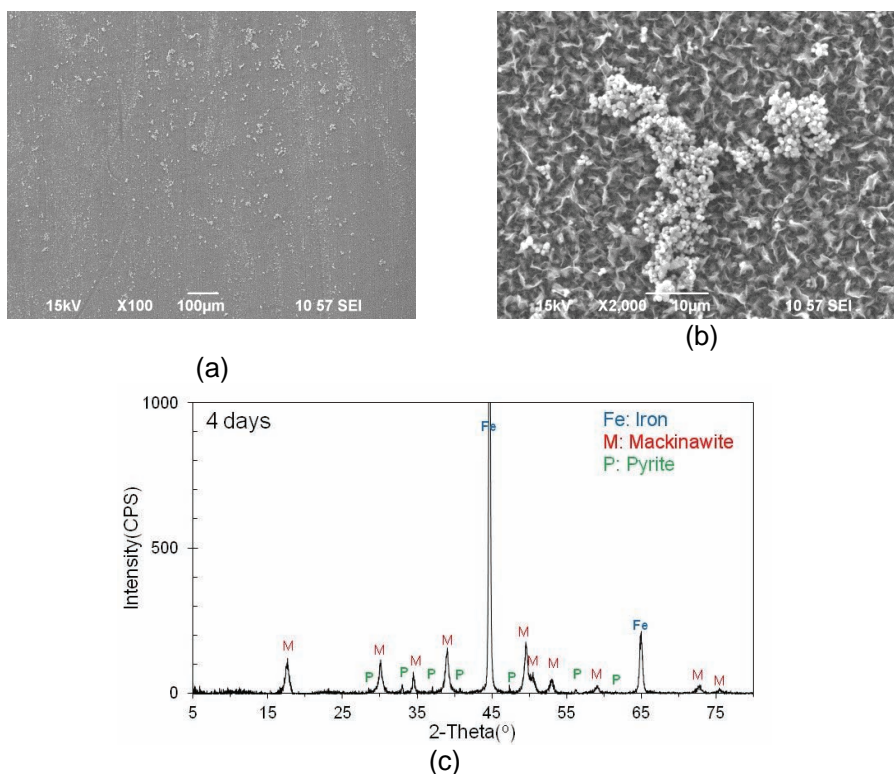


Figure 16. Corrosion product layer after 4 days of exposure at 80 °C: (a) SEM image of surface morphology with x 100 magnification; (b) SEM image of surface morphology with x 2,000 magnification; (c) XRD pattern.

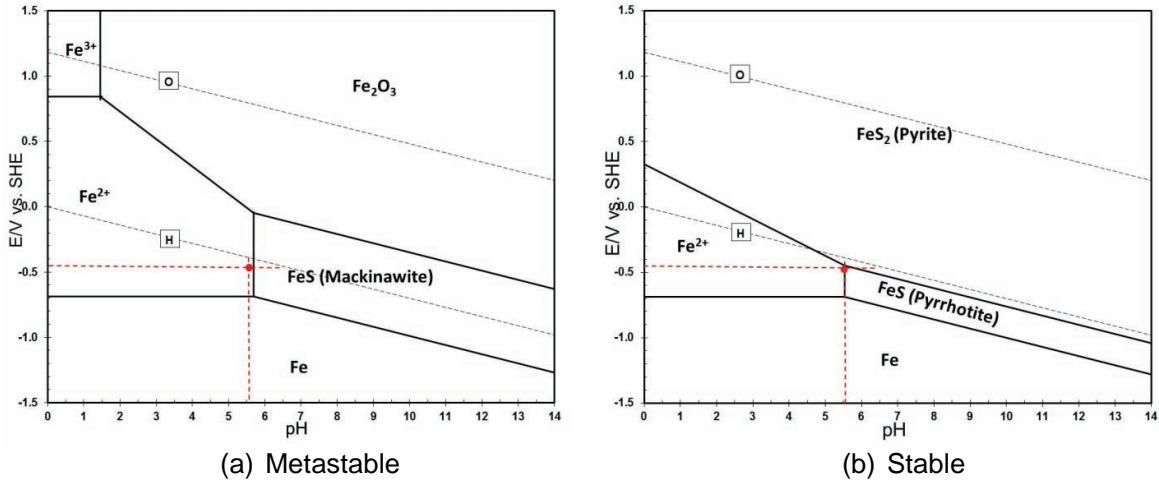
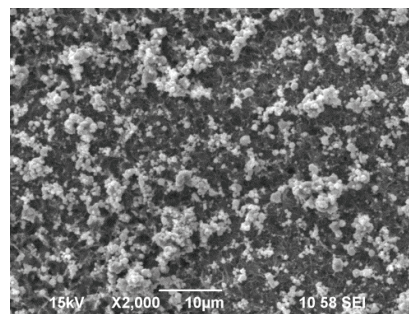
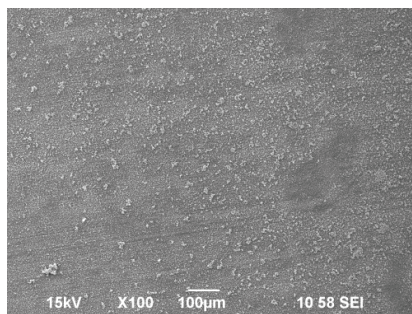


Figure 17. Verification of Pourbaix diagram after 4 days of exposure (Pourbaix diagram was generated at  $T = 80\text{ }^{\circ}\text{C}$ ,  $\text{pH}_2\text{S} = 0.053\text{ bar}$ ,  $[\text{Fe}^{2+}] = 0.045\text{ ppm}$ ,  $[\text{Fe}^{3+}] = 1.0 \times 10^{-6}\text{ M}$ ): (a) Mackinawite; (b) Mackinawite / Greigite / Pyrrhotite / Pyrite.

### Results after 7 days of exposure

The surface morphologies and composition of the corrosion product layer on the steel surface after 7 days of exposure are shown in Figure 18. The appearance is similar to the result from 4 days of exposure shown in Figure 16. The major difference is the quantities of the different iron sulfide phases. The SEM images in Figure 18 show more cubic crystals in lighter color on the steel surface compared to the previous 4-day sample, which is probably due to the increase in the amount of the pyrite phase. The growth of the pyrite phase is proved by the quantitative analysis of the corrosion product layer presented in Table 3. Comparing with the sample after 4 days, the percentage of pyrite grew from 2 % to 17 %. This growth is significant, and may suggest rapid kinetics of the growth of pyrite crystal after the nucleation. In contrast, the pyrrhotite phase is reported to nucleate quickly but grow sluggishly, which is also detected, changing from 3 % after 4 days to 9 % after 7 days. At the same time, the percentage of mackinawite decreases from 34% to 30%.

The formation of different phases of iron sulfide can be predicted with the Pourbaix diagrams generated at corresponding experimental conditions, shown in Figure 19. The experimental data point in Figure 19 (a) is a little left to the boundary of mackinawite formation, which could again be indicating the transformation of mackinawite into pyrite and pyrrhotite. The experimental data point in Figure 19 (b) is close to the “triple point” where all three phases: mackinawite, pyrite and pyrrhotite are stable confirming XRD findings. Generally, it can be concluded that at 80 °C the calculated Pourbaix diagrams are in reasonable agreement with the experimental results, confirming their validity. Furthermore, Pourbaix diagrams offered complementary information to those obtained by electrochemical and analytical techniques, thereby improving our understanding of the complex evolution of the corrosion process under conditions where different iron sulfide polymorphs form.



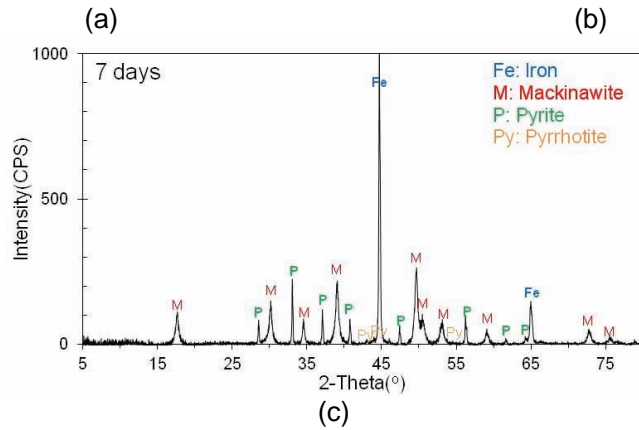


Figure 18. Corrosion product layer after 7 days of exposure at 80 °C: (a) SEM image of surface morphology with x 100 magnification; (b) SEM image of surface morphology with x 2,000 magnification; (c) XRD pattern.

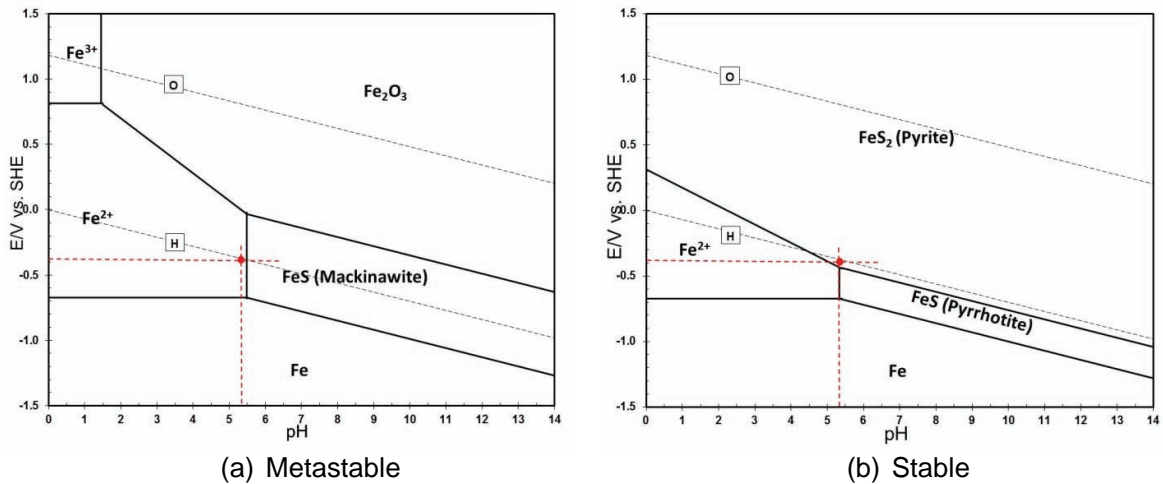


Figure 19. Verification of Pourbaix diagram after 7 days of exposure (Pourbaix diagram was generated at  $T = 80\text{ °C}$ ,  $p\text{H}_2\text{S} = 0.053\text{ bar}$ ,  $[\text{Fe}^{2+}] = 0.115\text{ ppm}$ ,  $[\text{Fe}^{3+}] = 1.0 \times 10^{-6}\text{ M}$ ): (a) Mackinawite; (b) Mackinawite / Greigite / Pyrrhotite / Pyrite.

Table 3 XRD quantitative analysis of the formed corrosion products layer at 80 °C.

Phases	Iron	Mackinawite	Pyrrhotite	Greigite	Pyrite	Iron Carbide
After 4 days	55%	34%	3%	1%	2%	5%
After 7 days	39%	30%	9%	2%	17%	3%

## CONCLUSIONS

- A comprehensive thermodynamic model has been developed to predict corrosion products for an  $\text{H}_2\text{S}$ - $\text{H}_2\text{O}$ - $\text{Fe}$  system with the focus on the conditions typical for the oil and gas applications.
- Pourbaix diagrams for an  $\text{H}_2\text{S}$ - $\text{H}_2\text{O}$ - $\text{Fe}$  system generated by the thermodynamic model were experimentally validated. The corrosion products formed on the steel surface were predicted by the Pourbaix diagrams constructed for the experimental conditions and confirmed by XRD analysis.

- Mackinawite and pyrrhotite were detected as corrosion products in H<sub>2</sub>S corrosion of mild steel at 25 °C. Mackinawite, pyrrhotite, and pyrite were found at 80 °C.

## ACKNOWLEDGEMENTS

The authors would like to express sincere appreciation to the following industrial sponsors for their financial support and direction: Anadarko, Baker Hughes, BP, Chevron, Clariant Oil Services, CNPC Tubular Goods, ConocoPhillips, DNV GL, Hess, INPEX Corporation, M-I SWACO, Multi-Chem, Nalco Champion, Occidental Oil Company, Petrobras, Petroleum Development Oman, Petroleum Institute (GRC), Petronas, PTT, Saudi Aramco, Sinopec, TransCanada, TOTAL, and Wood Group Integrity Management.

The authors also appreciate the help offered at the Center for Electrochemical Engineering Research, Department of Chemical and Biomolecular Engineering at Ohio University, enabling the use of the XRD equipment. Last but not least, great thanks go to Cody Shafer for the assistance in constructing experimental set-up figure.

## REERENCES

1. S. Nešić, W. Sun, "Acid Gas Corrosion", in J. A. Richardson et al. Ed., *Shreir's Corrosion*, 2nd ed., vol. 2, (Elsevier, 2010) p. 1270.
2. S. N. Smith, M. Joosten, Corrosion/2006, Paper no. 06115 (Houston, TX: NACE, 2006).
3. Y. Zheng, B. Brown, S. Nešić, *Corrosion*, 70, 4 (2014): p. 351-365.
4. W. Sun, S. Nešić, *Corrosion* 65, 5 (2009): p. 291-307.
5. A. Anderko, P. McKenzie, R. D. Young, *Corrosion* 57, 3 (2001): p. 202-213.
6. Y. Zheng, J. Ning, B. Brown, S. Nešić, Corrosion/2014, Paper no. 3907 (Houston, TX: NACE, 2014).
7. W. Sun, S. Nesic, and S. Papavinasam, *Corrosion*, 64, 7 (2008): p. 586-599.
8. E. Abelev, J. Sellberg, T. A. Ramanarayanan, S. L. Bernasek, *J. Mater. Sci.* 44, (2009): p. 6167-6181.
9. S. Kapusta, D. Raghu, J. Richard, Corrosion/2008, paper no. 08641, (Houston, TX: NACE, 2008).
10. S. N. Smith, B. Brown, W. Sun, Corrosion/2011, Paper no. 11081 (Houston, TX: NACE, 2011).
11. S. M. Wilhelm, "Galvanic corrosion caused by corrosion products," in H. P. Hack, Ed., *Galvanic Corrosion, ASTM STP 978*, (American Society for Testing and Materials, Philadelphia, 1988) p. 23.
12. C. M. Menendez, V. Jovancicevic, S. Ramachandran, M. Morton, D. Stegmann, *Corrosion* 69, 2 (2013): p. 145-156.
13. E. D. Verink, JR., "Simplified procedure for constructing Pourbaix diagrams," in R. W. Revie, Ed., *Uhlig's Corrosion Handbook*, 3rd ed., (Hoboken, NJ: John Wiley & Sons Inc., 2011) p. 93-101.
14. J. Bouet, J. P. Brenet, *Corros. Sci.* 3 (1963): p. 51-63.
15. M. Ueda, *Corros. Eng.* 44, 3 (1995): p.159-174.
16. A. Anderko, P. J. Shuler, *Computers & Geosciences* 23, 6 (1997): p. 647-658.
17. A. Anderko, S. J. Sanders, R. D. Young, *Corrosion* 53, 1(1997): p. 43-53.
18. T. Tanupabrungsun, D. Young, B. Brown and S. Nešić, Corrosion/2012, Paper no. 1418 (Houston, TX: NACE, 2012).
19. E. H. Oelkers, H. C. Helgeson, E. L. Shock, D. A. Sverjensky, J. W. Johnson, V. A. Pokrovskii, *J. Phys. Chem. Ref. Data*, 24, 4 (1995):p.1401-1560.
20. M. H. Kaye, W. T. Thompson, "Computation of Pourbaix diagrams at elevated temperature," in R. W. Revie, Ed., *Uhlig's Corrosion Handbook*, 3rd ed., (Hoboken, New Jersey: John Wiley & Sons Inc., 2011) p. 111-122.
21. J. Ning, Y. Zheng, D. Young, B. Brown, S. Nešić, *Corrosion* 70, 4 (2014): p. 375-389.
22. F. Gronvold, E. F. Westrum, Jr., *Inorg. Chem.*, 1, 1, (1962): p. 36-48.
23. B. Brown, Ph. D. Dissertation, Ohio University, 2013.
24. D. Abayarathna, A. Naraghi, S. Wang, Corrosion/2005, Paper no. 05624 (Houston, TX: NACE, 2005).
25. W. Sun, S. Nesic, S. Papavinasam, *Corrosion*, 64, 7 (2008): p. 586-599.
26. J. Han, B. Brown, D. Young, S. Nesic, *J. Appl. Electrochem.*, 40 (2010): p. 683